Study on orthorhombic parameters for 3D elastic full waveform inversion

Ju-Won Oh and Tariq Alkhalifah, King Abdullah University of Science and Technology*

Summary

For a better understanding of the influence of the parameterizations on the multi-parameter full waveform inversion (FWI) for 3D elastic orthorhombic media, we analyze the virtual sources for each c_{ij} parameter. Because the virtual sources for c_{ij} parameters can be regarded as bases of the virtual sources for other parameterizations, the insights developed here explains many of the scattering phenomena of the different parameters. The resulting radiation patterns provide insights on which parameter set is the best in the multi-parameter FWI for 3D elastic orthorhombic media. In this study, we analyze the virtual source for each c_{ij} parameter as a linear combination of several moment tensors. After that, we analyze the strain fields deformed by incident waves as momenta of the virtual source and their influences on sensitivity kernels of each c_{ij} parameter.

Introduction

When exploring for oil and gas in complex geologic structures, accurate and reliable estimates of subsurface material parameters are important for seismic interpretation and reservoir characterization. Such reliable estimates are usually attainable using the proper physical description of the multi parameter nature of the Earth in full waveform inversion (FWI) (Gholami et al., 2013; Operto et al., 2013; Alkhalifah and Plessix, 2014; Oh and Min 2014). In reservoir regions such a description is provided by the 3D elastic orthorhombic anisotropic model representation of the medium. Such a medium representation, however, poses considerable challenge in FWI due to the large number of parameters needed to describe the medium, and the potential for tradeoff.

The most important issue in multi-parameter FWI is finding the optimal parameterization to describe the subsurface parameters and yet have a reasonably unique signature in the data. Analyzing the radiation pattern of each parameter reveals whether such a parameter has a unique region of influence in the data. However, finding the best parameterization through analyzing the radiation patterns of each parameter in the many possible parameterizations is difficult for 3D elastic orthorhombic media. The data is given by 3 components and depends on 9 c_{ij} parameters (for more details about c_{ij} parameter representation, refer to Tsvankin [1997]).

In this study, we analyze the virtual sources and sensitivity kernels of c_{ij} parameters as bases functions for any virtual source in 3D elastic orthorhombic media. We first show that the virtual sources of c_{ij} parameters can be expressed as a linear combination of simple body forces. After that, we analyze the strain fields as momenta of the virtual source and sensitivity kernels as direct model parameter updates. This approach provides reasonable insights for the complicated radiation pattern of each parameter in 3D elastic orthorhombic media.

Inverse problem

The objective function of the time-domain waveform inversion using the l_2 norm of residuals between modelled (u_s) and field (d_s) data can be expressed as

$$E(\mathbf{p}) = \int \left[d_s(r,t) - u_s(r,t,\mathbf{p}) \right]^2 dt \,, \tag{1}$$

with

$$u_s(r,t,\mathbf{p}) = \int G_s(r,t,\mathbf{p}) * f_s(t) dt \,, \tag{2}$$

where r, s and t denote the receiver, source and time, respectively; $\mathbf{p}$ represents the model parameter; $G_s(r,t,\mathbf{p})$ and $f_s(t)$ represent the Green's function from a source (s) to a receiver (r) and the seismic source function, respectively. The symbol, *, denotes the temporal convolution. Model parameters minimizing the objective function can be obtained by calculating the gradient of the objective function. The gradient with respect to the kth model parameter can be obtained as follows:

$$\frac{\partial E}{\partial p_k} = \sum_s \sum_r \left[\int J_{s,k}(r,t,\mathbf{p}) \times \left[d_s(r,t) - u_s(r,t,\mathbf{p}) \right] dt \right]. \tag{3}$$

$J_{s,k}(r,t,\mathbf{p})$ is the partial derivative wavefields (so-called Jacobian) with respect to the kth model parameter. As shown in eq. (3), the radiation patterns of partial derivative wavefields determine which parts of data we use to invert the parameter (p_k). For this reason, many previous studies (Operto et al. 2013; Alkhalifah and Plessix, 2014) are devoted to analyzing the radiation patterns of the partial derivative wavefields for each parameter.

Virtual sources for c_{ij} parameters

The elastic wave equation for 3D orthorhombic media can be expressed by

$$\begin{aligned} \rho \frac{\partial^2 u_x}{\partial t^2} = & \frac{\partial}{\partial x}\left[c_{11}\frac{\partial u_x}{\partial x} + c_{12}\frac{\partial u_y}{\partial y} + c_{13}\frac{\partial u_z}{\partial z} \right] \\ & + \frac{\partial}{\partial y}\left[c_{44}\left(\frac{\partial u_x}{\partial y} + \frac{\partial u_y}{\partial x} \right) \right] + \frac{\partial}{\partial z}\left[c_{55}\left(\frac{\partial u_x}{\partial z} + \frac{\partial u_z}{\partial x} \right) \right], \end{aligned} \tag{4}$$

$$\begin{aligned} \rho \frac{\partial^2 u_y}{\partial t^2} = & \frac{\partial}{\partial y}\left[c_{12}\frac{\partial u_x}{\partial x} + c_{22}\frac{\partial u_y}{\partial y} + c_{23}\frac{\partial u_z}{\partial z} \right] \\ & + \frac{\partial}{\partial x}\left[c_{44}\left(\frac{\partial u_x}{\partial y} + \frac{\partial u_y}{\partial x} \right) \right] + \frac{\partial}{\partial z}\left[c_{66}\left(\frac{\partial u_y}{\partial z} + \frac{\partial u_z}{\partial y} \right) \right], \end{aligned} \tag{5}$$

DOI http://dx.doi.org/10.1190/segam2015-5849903.1

and

$$\rho\frac{\partial^2 u_z}{\partial t^2}=\frac{\partial}{\partial z}\left[c_{31}\frac{\partial u_x}{\partial x}+c_{23}\frac{\partial u_y}{\partial y}+c_{33}\frac{\partial u_z}{\partial z}\right]+\frac{\partial}{\partial x}\left[c_{55}\left(\frac{\partial u_x}{\partial z}+\frac{\partial u_z}{\partial x}\right)\right]+\frac{\partial}{\partial y}\left[c_{66}\left(\frac{\partial u_y}{\partial z}+\frac{\partial u_z}{\partial y}\right)\right], \quad (6)$$

where u_x, u_y and u_z are the displacement fields along x, y and z directions, respectively. The above elastic wave equations can be expressed in following matrix form:

$$\mathbf{Su}=\mathbf{f} \quad . \quad (7)$$

The terms **S**, **u** and **f** denote the modelling operator, displacement vector and seismic source, respectively. If we take the partial derivative of eq. (7) with respect to each c_{ij} parameter, the partial derivative wavefields, *J*, in eq. (3) can be expressed as follows:

$$\frac{\partial \mathbf{u}}{\partial c_{ij}}=\mathbf{S}^{-1}\mathbf{f}^{v}_{c_{ij}}, \quad (8) \quad \text{where} \quad \mathbf{f}^{v}_{Cij}=-\frac{\partial \mathbf{S}}{\partial c_{ij}}\mathbf{u}. \quad (9)$$

We notice that the elastic wave equation for the partial derivative wavefields in eq. (8) resembles the original elastic wave equation in eq. (7). This is why we call the source in eq. (9) as a virtual source.

Based on the fact that the partial derivative wavefields are scattered wavefields generated by a point perturbation, where we want to estimate (so-called virtual source), Oh and Min (2014) tried to analyze the behavior of the virtual source for each parameter. They decomposed the virtual source to their bases terms and suggested 10 possible terms to represent the virtual source for 2D elastic VTI media, so-called basis virtual source. This provides a useful tool to understand the source mechanism of the virtual source in the elastic media, as these basis terms are with respect to a given directional derivative. However, based on their decomposition approach of the virtual source, we end up with 28 basis virtual sources in 3D elastic orthorhombic media. Because of this large number of basis virtual sources, it would be difficult to interpret the physical behaviors of the virtual sources for each parameter in 3D elastic orthorhombic media. Therefore, we need to reorganize the concept of the basis virtual source because many basis virtual sources are usually combined together as they appear in many terms. We notice that, in a practical point of view, the virtual sources for c_{ij} parameters can be regarded as bases of the virtual source for any kind of parameter combination. This is because the virtual sources for each c_{ij} parameter cannot be split over the parameterization. In other words, the virtual source for any parameter in 3D elastic media can be expressed by the linear combination of the virtual sources for c_{ij} parameters. We also notice that the virtual source for c_{ij} parameters can be expressed as a linear combination of the basis virtual sources suggested by Oh and Min (2014). From such observations, we express the virtual sources for the c_{ij} parameter as a linear combination of four moment tensors given by:

$$\mathbf{f}^{v}_{Cij}=\mathbf{M}^{\text{explosive}}\begin{pmatrix}w_x\\w_y\\w_z\end{pmatrix}+w_{xy}\mathbf{M}^{DC}_{xy}+w_{xz}\mathbf{M}^{DC}_{xz}+w_{yz}\mathbf{M}^{DC}_{yz} \quad (10)$$

where

$$\mathbf{M}^{\text{explosive}}=\begin{pmatrix}1&0&0\\0&1&0\\0&0&1\end{pmatrix} \quad (11) \qquad \mathbf{M}^{DC}_{xy}=\begin{pmatrix}0&1&0\\1&0&0\\0&0&0\end{pmatrix} \quad (12)$$

$$\mathbf{M}^{DC}_{xz}=\begin{pmatrix}0&0&1\\0&0&0\\1&0&0\end{pmatrix} \quad (13) \qquad \mathbf{M}^{DC}_{yz}=\begin{pmatrix}0&0&0\\0&0&1\\0&1&0\end{pmatrix} \quad (14)$$

M is a 3×3 moment tensor whose diagonal elements indicate tensile forces (or compressional forces depending on the sign) and off-diagonal elements denote a couple of shear forces as expressed by Jost and Herrmann (1989). The main advantage of this approach is that the radiation patterns of c_{ij} parameters for 3D elastic orthorhombic media, which are very complicated, can be decomposed into several familiar radiation patterns as shown in Figure 1. The first one ($\mathbf{M}^{\text{explosive}}$) is a combination of simple tensile forces and the others ($\mathbf{M}^{DC}_{xy}$, $\mathbf{M}^{DC}_{xz}$ and $\mathbf{M}^{DC}_{yz}$) denote double coupled forces, whose radiation patterns are also well-known in earthquake seismology (Mussett and Khan, 2000) because they represent faulting mechanisms.

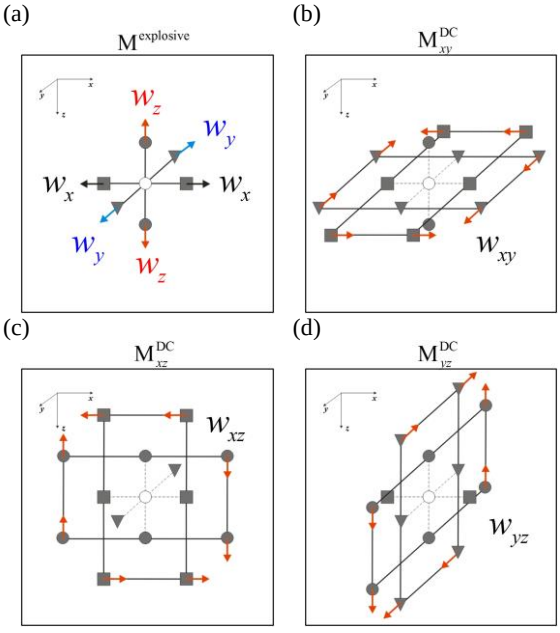

Figure 1: Moment tensor descriptions of four virtual source groups for c_{ij} parameters: (a) explosive source ($\mathbf{M}^{\text{explosive}}$) and double coupled (DC) sources acting on (b) xy plane ($\mathbf{M}^{DC}_{xy}$), (c) xz plane ($\mathbf{M}^{DC}_{xz}$) and (d) yz plane ($\mathbf{M}^{DC}_{yz}$).

DOI http://dx.doi.org/10.1190/segam2015-5849903.1

Characteristics of the FWI for c_{ij} parameter

In this section, we analyze the characteristics of FWI for each c_{ij} parameter in terms of their momenta and sensitivity kernels. As Oh and Min (2014) showed, the analysis for strain fields deformed by incident waves provides good insights for the spatial coverage of the FWI for each parameter because the strains act as momenta of the virtual source. On the other hand, the analysis for the sensitivity kernel (Woodward, 1992) helps us understand the characteristics of the FWI for each parameter because they reflect the model parameter update directly.

For numerical simulations, we use the 3D 4th-order staggered grid finite difference method (refer to Graves, 1996) with CPML boundaries (Komatitsch and Martin, 2007). We modeled 6 km × 6 km × 3 km with a uniform grid spacing of 20 m. The source wavelet is a first derivative of the Gaussian function, in which the dominant frequencies are given by10 Hz and 2.5 Hz, respectively.

Table 1: Coefficients of nine c_{ij} parameters for eq. (10)

Coefficients	w_x	w_y	w_z	w_{xy}	w_{xz}	w_{yz}
c_{11}	$\frac{\partial u_x}{\partial x}$	0	0	0	0	0
c_{12}	$\frac{\partial u_y}{\partial y}$	$\frac{\partial u_x}{\partial x}$	0	0	0	0
c_{13}	$\frac{\partial u_z}{\partial z}$	0	$\frac{\partial u_z}{\partial x}$	0	0	0
c_{22}	0	$\frac{\partial u_y}{\partial y}$	0	0	0	0
c_{23}	0	$\frac{\partial u_z}{\partial z}$	$\frac{\partial u_y}{\partial y}$	0	0	0
c_{33}	0	0	$\frac{\partial u_z}{\partial z}$	0	0	0
c_{44}	0	0	0	$\frac{\partial u_x}{\partial y}+\frac{\partial u_y}{\partial x}$	0	0
c_{55}	0	0	0	0	$\frac{\partial u_x}{\partial z}+\frac{\partial u_z}{\partial x}$	0
c_{66}	0	0	0	0	0	$\frac{\partial u_y}{\partial z}+\frac{\partial u_z}{\partial y}$

In eq. (10), the coefficients, which are listed on Table 1, determine the combination and the momenta of the aforementioned four body forces for the virtual source of each c_{ij} parameter. In 3D elastic orthorhombic media, we notice that all normal and shear strains can be regarded as momenta for the virtual source of each c_{ij} parameter. Figure 2 shows the 6 types of strain fields deformed by incident waves that are generated by the vertical body force at the middle of the surface. The momenta of the virtual sources for c_{11}, c_{22} and c_{33} are normal strains along x, y and z direction, respectively. From Figure 2, we observe that horizontal normal strains have dominant directivity along each horizontal axis, but the vertical normal strain is dominant along the vertical axis. On the other hand, most deformations caused by strong surface waves occurred near the surface for shear strains. This behavior of the strain fields affect the sensitivity kernels acting as momenta of the virtual source.

Figure 3 shows the sensitivity kernels obtained for each c_{ij} parameter. For visualization, we use different scale for each parameter. As we can guess from eq. (10), the shape of sensitivity kernels for each parameter is determined by the types of body forces (Figure 1) and their momenta (Figure 2) depending on the combination shown in Table 1. As a result, some parameters such as c_{11}, c_{22}, c_{12} have small model update along vertical direction from the source. This is because their virtual sources are derived from horizontal normal strains and are not good to recover deep structures. The sensitivity kernel for c_{33} shows relatively large model updates along vertical direction that might be good for the deep structure. For c_{13}, we also observe strong reverse updates near the surface, which is caused by reverse particle motions of S-S scattered waves (Oh and Min, 2015). We also observe very large model updates due to strong surface waves near surface, particularly in c_{44}, c_{55} and c_{66}. For this reason, we require accurate shallow structures prior to the FWI to reveal deeper structures.

Conclusions

We analyzed the virtual source of the partial derivative wavefields for c_{ij} parameters in 3D elastic orthorhombic media. Because the virtual source of c_{ij} parameters in 3D elastic orthorhombic media cannot be split over the parameterization, the virtual source of c_{ij} parameters can be regarded as bases for the virtual source of any parameter representation. The expression of the virtual source for the c_{ij} parameters using 4 types of body forces provides fundamental information related to the radiation patterns of each c_{ij} parameter. The analyses for the strain fields deformed by the incident wave showed that various types of strains act as momenta of the virtual source. The normal strains have dominant directivity depending on the direction of the deformation. On the other hand, we observed large amounts of deformation generated by strong surface wave in shear strains. Finally, these characteristics of each strain affect the shape of sensitivity kernels for each c_{ij} parameter. The sensitivity kernels showed that each parameter has limited spatial coverage. In addition, good initial models for near surface structures will be required for the estimation of deep structures because of large model updates caused by surface waves. We expect that this study can provide a good framework to analyze the sensitivity of FWI to numerous parameterizations for 3D elastic orthorhombic media, in which we plan to share some of them in the presentation.

Acknowledgments

We thank King Abdullah University of Science and Technology (KAUST) for the financial support.

DOI http://dx.doi.org/10.1190/segam2015-5849903.1

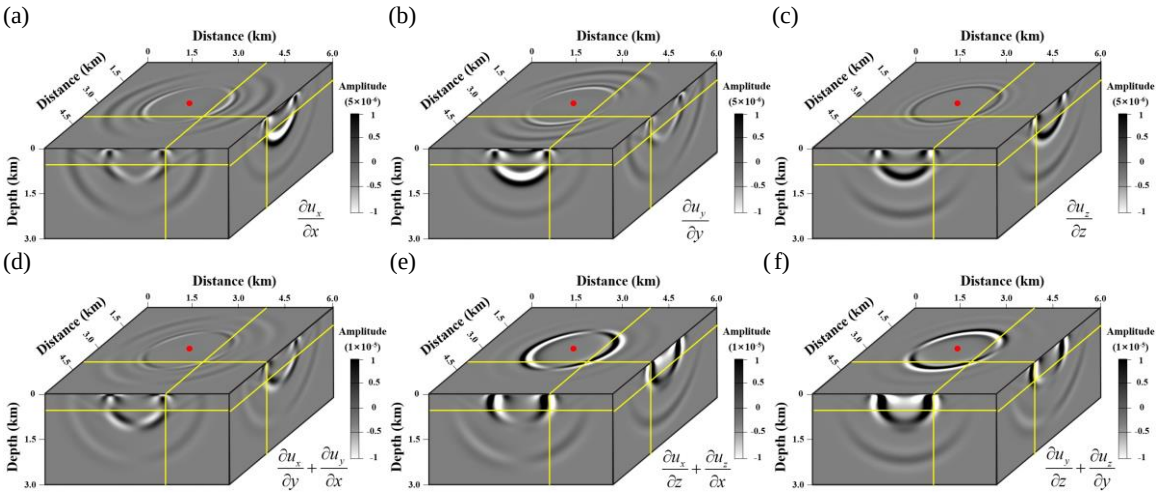

Figure 2: Snapshots of normal strains along (a) x-direction, (b) y-direction and (c) z-direction and shear strains on (d) xy-plane, (e) xz-plane and (f) yz-plane at 0.6 s. The red circle indicates the seismic source that acts as a vertical body force. The yellow lines denote the location of each plane.

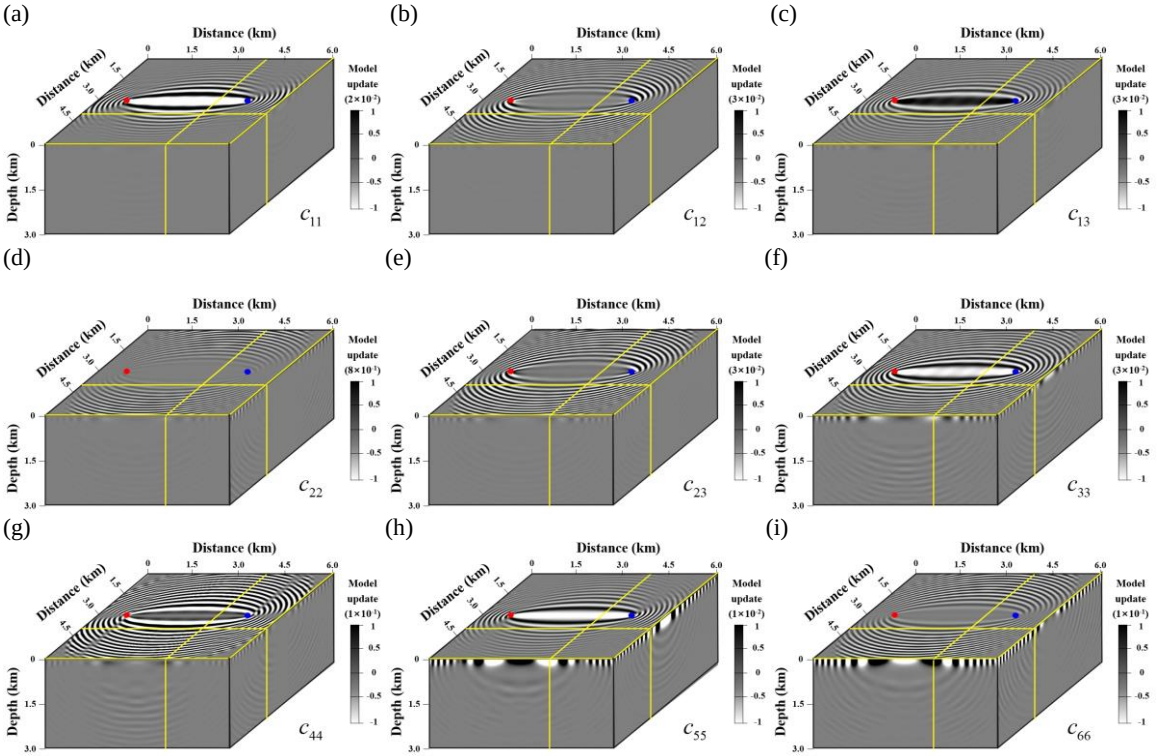

Figure 3: The model update responses (sensitivity kernels) for the (a) c_{11}, (b) c_{12}, (c) c_{13}, (d) c_{22}, (e) c_{23}, (f) c_{33}, (g) c_{44}, (h) c_{55} and (i) c_{66} perturbations for a monochromatic wavefield of 5 Hz. The red and blue circles denote the source and receiver positions, respectively. The yellow lines denote the location of each plane.

DOI http://dx.doi.org/10.1190/segam2015-5849903.1

EDITED REFERENCES

Note: This reference list is a copyedited version of the reference list submitted by the author. Reference lists for the 2015 SEG Technical Program Expanded Abstracts have been copyedited so that references provided with the online metadata for each paper will achieve a high degree of linking to cited sources that appear on the Web.

REFERENCES

Alkhalifah, T., and R.-E. Plessix, 2014, A recipe for practical full-waveform inversion in anisotropic media: An analytical parameter resolution study: Geophysics, **79**, no. 3, R91–R101.

Gholami, Y., R. Brossier, S. Operto, A. Ribodetti, and J. Virieux, 2013, Which parameterization is suitable for acoustic vertical transverse isotropic full waveform inversion? Part 1: Sensitivity and trade-off analysis: Geophysics, **78**, no. 2, R81–R105, http://dx.doi.org/10.1190/geo2012-0204.1.

Graves, R. W., 1996, Simulating seismic wave propagation in 3D elastic media using staggered-grid finite differences: Bulletin of the Seismological Society of America, **86**, no. 4, 1091–1106.

Jost, M. L., and R. B. Herrmann, 1989, A student's guide to and review of moment tensors: Seismological Research Letters, **60**, 37–57.

Komatitsch, D., and R. Martin, 2007, An unsplit convolutional perfectly matched layer improved at grazing incidence for the seismic wave equation: Geophysics, **72**, no. 5, SM155–SM167, http://dx.doi.org/10.1190/1.2757586.

Mussett, E. A., and M. A. Khan, 2000, Looking into the earth: An introduction to geological geophysics: Cambridge University Press, http://dx.doi.org/10.1017/CBO9780511810305.

Oh, J. W., and D. J. Min, 2014, Multi-parametric FWI using a new parameterisation for elastic VTI media: 76th Conference & Exhibition, EAGE, Extended Abstracts, doi:10.3997/2214-4609.20141084.

Oh, J. W., and D. J. Min, 2015, A two-stage elastic FWI strategy for 2D VTI elastic media to improve c13 structure: 77th Conference & Exhibition, EAGE, Extended Abstracts, http://dx.doi.org/10.3997/2214-4609.201413408.

Operto, S., Y. Gholami, V. Prieux, A. Ribodetti, R. Brossier, L. Métivier, and J. Virieux, 2013, A guided tour of multiparameter full-waveform inversion with multicomponent data: From theory to practice: The Leading Edge, **32**, 1040–1054.

Tsvankin, I., 1997, Anisotropic parameters and P-wave velocity for orthorhombic media: Geophysics, **62**, 1292–1309, http://dx.doi.org/10.1190/1.1444231.